Journal of the Iranian Chemical Society (2021) 18:1231–1241
https://doi.org/10.1007/s13738-020-02106-7

ORIGINAL PAPER

Experimental and theoretical studies of a novel synthesized azopyrazole-benzenesulfonamide derivative as an efficient corrosion inhibitor for mild steel

M. A. Mostfa[1] · H. Gomaa[1] · Ismail M. M. Othman[1] · Gomaa A. M. Ali[1]

Received: 11 September 2020 / Accepted: 15 October 2020 / Published online: 31 October 2020

Abstract

Herein, a novel inhibitor for the mild steel corrosion in an acidic environment based on azopyrazole-benzenesulfonamide derivative, namely 4-(2-(3-methyl-5-oxo-1-tosyl-1H-pyrazol-4(5H)-ylidene) hydrazinyl)-*N*-(pyrimidin-2-yl) benzenesulfonamide, is investigated. The electrochemical tests were performed using open-circuit potential, potentiodynamic polarization, and electrochemical impedance spectroscopy. Furthermore, the corrosion inhibition mechanism is explained using Tafel polarization and Langmuir isotherm. The obtained findings revealed that corrosion resistance effectiveness increased as the resistant concentration grows. Moreover, Tafel polarization diagrams indicated that the compound used is a mixed-form inhibitor. The chemically quantum factors have been determined using the density functional hypothesis. A good correlation between the experimental findings and theoretical predictions is found from all the results of this study. In addition, the proposed corrosion inhibitor can be used for a wide range of industrial applications due to the high inhibition efficiency.

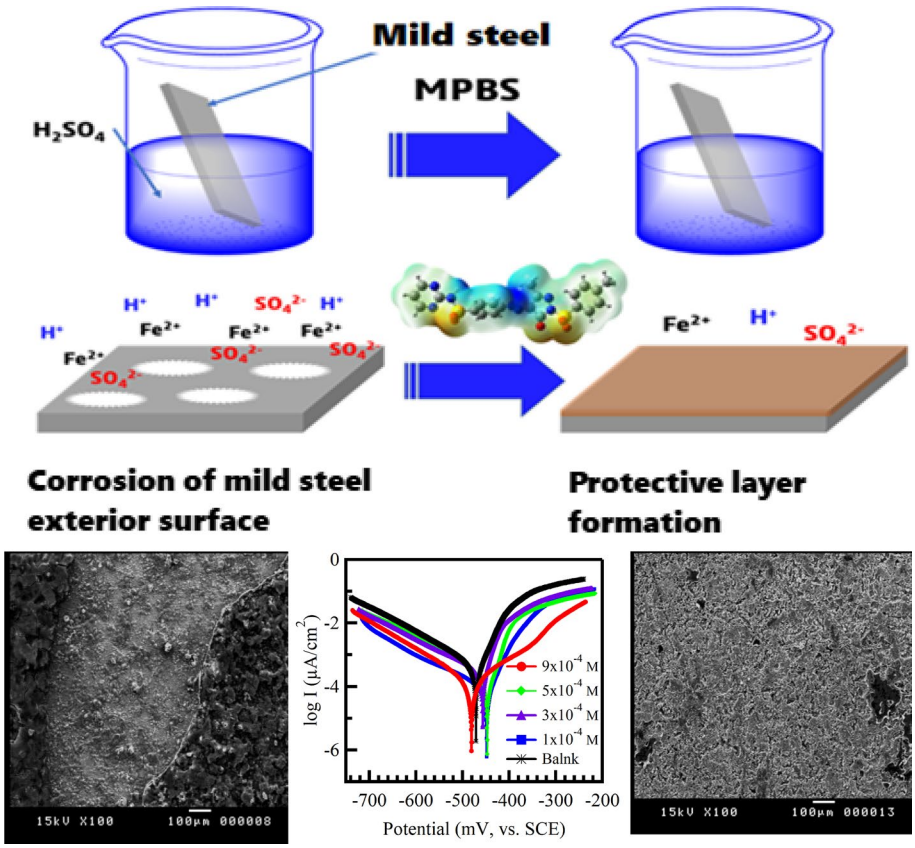

Extended author information available on the last page of the article

Keywords Corrosion inhibitor · Organic inhibitor · Mild steel · Azopyrazole-benzenesulfonamide · Density functional theory

Introduction

Corrosion is the damaging effect of metals through chemical or electrochemical reactions with their surrounding environment [1, 2]. Spontaneous dissolution of mild steel in acidic environments presents a dilemma in using steel in storing-containers and oil refineries, and other industrial applications. That is because the acid solutions are commonly employed to get rid of the unwanted scale and rust in many industrial processes [3, 4]. Industrial processes operating in an acidic medium are most vulnerable to metal loss by corrosion, resulting in a substantial economic loss and restraining technological progress [5–7]. Some organic inhibitors are either toxic or have an environmental concern [8–10]. On the other hand, nontoxic inhibitors are promising candidates for corrosion protection. Azopyrazole-benzenesulfonamide derivative has biological properties, including antitumor activity, highly effective antimicrobial, and antitubercular [11–13]. Pyrazole derivatives are among the most heterocyclic compounds that work by adsorption on metal-surface through nitrogen atoms, other than by triple or consecutive double-bonds or aromatic rings in their chemical structures. Various heterocyclic materials were used for the corrosion inhibition of mild steel in acidic media, such as pyrrole, imidazoline, pyridine, triazole, and pyrimidine [14–17]. Experimental methods help clarify the procedure of the corrosion suppression process, although these methods are often time-consuming. Recently, hardware and software-programs developments have commenced the efficient utilization of chemical theoretic calculations in corrosion inhibition investigations. They also serve to understand the connection between corrosion repression efficacy and molecular properties of the inhibitor [18–20].

In this work, the azopyrazole-benzenesulfonamide derivative has been investigated using various electrochemical methods as a new corrosion inhibitor for mild steel in acidic media. The efficacy has been correlated with the chemically quantum factors.

Materials and methods

Inhibitor preparation

The 4-(2-(3-methyl-5-oxo-1-tosyl-1H-pyrazol-4(5H)-ylidene) hydrazinyl)-*N*-(pyrimidin-2-yl) benzenesulfonamide (MPBS) inhibitor has been synthesized according to the procedure reported in our previous work [21]. Briefly, a solution of 3-methyl-1-tosyl-1H-pyrazol-5(4H)-one [22] (10 mmol) and sodium acetate (2 g(in ethanol (20 mL) was treated with the appropriate diazonium salt of sulfadiazine (10 mmol). This salt was preciously prepared by diazotizing a solution of 4-amino-*N*-(pyrimidin-2-yl)benzenesulfonamide (10 mmol) in HCl (1.5 mL) with a solution of $NaNO_2$ (10 mmol) in 5 mL water in an ice bath according to the scheme presented in our previous work [21].

Electrochemical measurements

Mild steel plates (sizes $5.0 \times 1.0 \times 0.1$ cm) were supplied by AL-EZZ Company, Alexandria, Egypt. The steel composition was Fe (98.74%), Mn (0.71%), Cu (0.182%), C (0.17%), Ni (0.072%), Cr (0.045%), Si (0.022%), F (0.022%), Al (0.0017%), Sn (0.011%), Mo (0.011%), and P (0.010%) mass percentage. Before the test, the plates were manually sanded using emery paper (SiC paper up to 1000 and 1400 grade) to obtain a mirror finish surface. Specimens were then washed by acetone and dried with air before dipping in the trial/test solution.

A 1.0 mol/LH_2SO_4 solution is prepared from a 95–98% concentrated solution (Sigma-Aldrich Laborchemikalien, German) and used as a corrosive medium. The inhibitor used herein at concentrations from 1×10^{-4} to 9×10^{-4} M was prepared in 1.0 M sulfuric acid solutions at 30 °C.

The corrosion cell used in this study consists of three electrodes, mild steel as a working/employed electrode, Pt wire as a counter electrode, and saturated calomel as a reference electrode. The exposed surface domain of the employed electrode is 1.0×1.0 cm.

The electrochemical behavior of the mild steel sample in 1.0 mol/LH_2SO_4 solution at various concentrations of MPBS corrosion inhibitor at 30 °C was researched applying open-circuit potential (OCP) for 30 min to an equilibrium state was achieved. Potentiodynamic polarization tests were performed to estimate Tafel slopes using the EG&G potentiostat/galvanostat version 273A with corrosion analysis software 352/252 2.01 (Princeton Applied Research, USA). The linear polarization (LP) was calculated from – 20 to + 20 mV versus corrosion potential (E_{corr}). The Tafel plots (TP) were traced from –250 to + 250 mV versus E_{corr}. The scanning rates for LP and TP were 0.166 and 0.4 mV/s, respectively [23]. In the existence and non-existence of the MPBS inhibitor, electrochemical impedance spectroscopy (EIS) was utilized to examine the attitude of mild steel after 2 h of inundation. A sinusoidal voltage signal of 10 mV was operated in a frequency limit of 10^5 to 10^{-3} Hz. EIS measurements were taken with an AUTO AC DSP device (ACM

Instruments) device. All impedance analyses were done at the open-circuit potential and 30 °C [24].

Morphological study

A scanning electron microscope (SEM) is employed to investigate the exterior surface morphology and topology of mild steel in the presence and absence of the inhibitor. SEM was assessed using JEOL (JEOL Ltd, Tokyo, Japan) JSM 5400 LV scanning microscope.

Quantum calculations

Quantum chemical estimations were achieved using the Gaussian 09 W program. Molecular geometries of the studied MPBS inhibitor were optimized with B3LYP/6-311G (*d*, *p*) [25, 26]. The chemical quantum factors such as the highest occupied molecular orbital energy (E_{HOMO}), lowest unoccupied molecular orbital energy (E_{LUMO}), energy gap (ΔE), electron affinity (EA), ionization potential (IP), electronegativity (χ), global hardness (η), softness (σ), electrophilicity index (ω), dipole moment (Dm), total energy (TE) and the fraction of electrons transferred (ΔN) were considered as the following Eqs. (1)–(8) [27–31]:

$$\Delta E = E_{LUMO} - E_{HOMO} \tag{1}$$

$$EA = -E_{LUMO} \tag{2}$$

$$IP = -E_{HOMO} \tag{3}$$

$$x = \frac{IP + EA}{2} \tag{4}$$

$$\eta = \frac{IP - EA}{2} \tag{5}$$

$$\sigma = \frac{1}{\eta} \tag{6}$$

$$\omega = \frac{x^2}{\eta} \tag{7}$$

$$\Delta N = \frac{\left[x^{Fe} - x^{inh}\right]}{2\left[\eta^{Fe} + \eta^{inh}\right]} \tag{8}$$

In Eq. (8), theoretical electronegativity and hardness values for iron were taken as ($\chi^{Fe} \approx 7$ eV and as $\eta^{Fe} = 0$) [32]. The maps of molecular electrostatic potential (MEP) and their contours were calculated to determine electrophilic and nucleophilic sites on the inhibitor's surface.

Results and discussion

Structural characteristics of the synthetic inhibitor

Full characterization data of the prepared inhibitor, including FTIR, ^{1}HNMR, ^{13}CNMR, and elemental analysis (C, H, N, S), are presented and discussed in detail in our previous work [21]. FTIR spectra illustrated the active groups predicted in the fabricated compound inhibitor, as listed in Table 1. ^{1}HNMR data indicated the distribution of hydrogen H^+ in the synthesized inhibitor. ^{13}CNMR spectra indicated the expected distribution of carbon atoms within the synthesized inhibitor. In addition, Table 1 shows the elemental composition (C, H, N, and S) indicated that approximately the elemental percentage of the theoretic and real data for each element is closed, proving that the proposed inhibitor is prepared with a high grade of purity.

Electrochemical measurements

Figure 1a illustrates the variation of the OCP of the mild steel electrode was submerged for 30 min in 0.1 M sulfuric acid as well as in the existence of numerous concentrations of corrosion inhibitor at 30 °C to establish steady state (OCP). After measuring the steady state (OCP) for blank solution shifts to a slightly negative potential than the immersion potential values, that indicates the destruction of pre-immersion oxide film on the electrode surface [32]. When different concentrations of MPBS are added as an inhibitor to the aggressive medium, values of steady state (OCP) shift towards positive direction of potential than the steady state (OCP) of blank, due to the formation of an outer-layer of MPBS inhibitor molecules on the mild steel exterior-surface which effect directly on the anodic corrosion reaction [33].

Table 1 FTIR bands and elemental analysis (C, H, N, and S) of the synthesized MPBS inhibitor

FTIR band	Wavenumber (cm^{-1})	Element	Detected ratio (%)	Calculated ratio (%)
(2NH)	3346, 3261	C	49.11	49.32
Symmetric and symmetric stretching (CH)	2977	H	3.73	3.94
(C=O)	1682	N	19.09	19.31
(C=N)	1612	S	12.49	12.71
(C=C) aromatic ring stretching	1507			
($2SO_2$) stretching	1219, 1118			

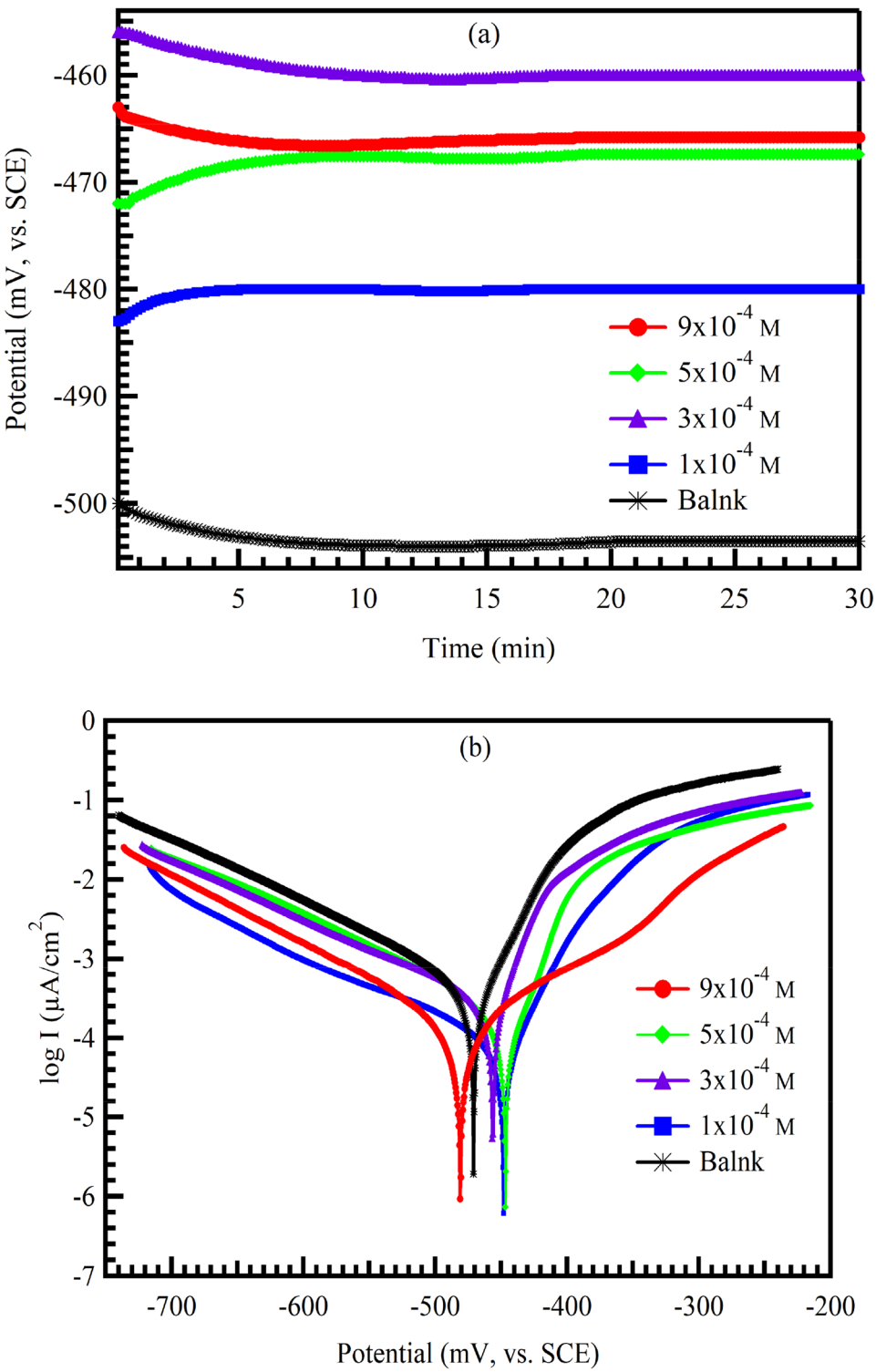

Fig. 1 Potential time (**a**) and Tafel polarization (**b**) curves for mild steel in 1.0 mol/L H_2SO_4 containing various concentrations of MPBS inhibitor at 30 °C

Linear and Tafel polarization techniques provide two methods for measuring the corrosion rate (CR) of the studied metal electrode. The LP values were obtained from the current I (μA/cm^2)/potential E (mV) plots at free corrosion potential. The values of the polarization resistance (R_p), the inhibition efficiency ($\eta p\%$), and the corrosion current density (I_{corr}) are listed in Table 2. The findings revealed that R_p and ηp increased, and I_{corr} decreased with increasing the inhibitor concentration in blank solution at 30 °C. This indicates that MPBS acts as a suitable inhibitor due to creating a layer on the metal exterior-surface [34]. The Tafel plots of the mild steel corrosion without and with

Table 2 Potentiodynamic factors for mild steel in 1.0 mol/L H_2SO_4 containing various concentrations of MPBS inhibitor at 30 °C

Test solution	Conc. (M)	R_P (Ω)	β_a (mV/dec)	β_c (mV/dec)	$-E_{corr}$ (mV)	I_{corr} (μA/cm^2)	CR (mpy)	ηp (%)	Surface coverage (θ)
Blank	–	42.15	230.58	221.21	473	669.01	616.85	-	-
MPBS	1×10^{-4}	59.12	162.66	233.28	455	303.21	279.57	57.77	0.58
	3×10^{-4}	65.58	140.34	200.51	466	220.33	203.15	69.31	0.69
	5×10^{-4}	72.59	93.52	188.98	456	155.99	143.83	78.27	0.78
	9×10^{-4}	86.63	81.02	119.26	464	45.88	42.30	93.61	0.94

MPBS compound concentrations varied from 1×10^{-4} to 9×10^{-4} M are exhibited in Fig. 1b. The polarization data, such as corrosion potential (E_{corr}), cathodic (β_c) and anodic (β_a) Tafel slopes, CR, ηp, and coverage surfaces (θ), are obtained from Tafel polarization curve extrapolation [31, 35, 36]. These parameters are listed in Table 2. The CR, ηp and θ are calculated using Eqs. (9)–(11).

$$\mathrm{CR} = 0.13 I_{corr} \frac{(\mathrm{Eq}\cdot\mathrm{Wt})}{A\cdot d} \tag{9}$$

$$\eta p\% = \left[\frac{\left(\mathrm{CR}_{uninh} - \mathrm{CR}_{inh}\right)}{\mathrm{CR}_{inh}}\right] \tag{10}$$

$$\theta = \frac{\eta p\%}{100} \tag{11}$$

where Eq·wt is the metal equivalent mass, A is the area (cm^2), d is density (g/cm^3), and 0.13 is the time conversion factor. CR_{uninh} and CR_{inh} are the corrosion rates in the absence and existence of the proposed corrosion inhibitor. The values of Tafel slopes are markedly changed in the existence of various concentrations of MPBS as a corrosion inhibitor. These results reflect the effect of MPBS on both the anodic and cathodic reactions and thus are deemed to be a mixed type inhibitor for mild steel electrode in 1.0 mol/L H_2SO_4 [37, 38]. The gained results in Table 2 exhibited that the CR of mild steel in the deficiency of MPBS corrosion inhibitor increased steeply, whereas the CR increases slowly in the present concentrations of MPBS compound as an inhibitor [39]. The corrosion repression efficiency values rise in the presence of MPBS inhibitor, and protective action can be assigned to the electron density. This electron density differs with the substituents in the inhibitor molecules. The nitrogen can more easily provide an unmarried couple of electrons to the mild steel surface and thus reduce corrosion rate [40]. Table 2 indicates better MPBS at 30 °C ($\eta p = 93.61\%$ at 9×10^{-4} M) due to high molecular weight (513.09 gm) and presence of S, N, O, and aromatic rings, which have the ability to adsorption and formation of shielding and protecting layers on the mild steel surface.

Electrochemical impedance spectroscopy has many advantages over other electrochemical methods in studying corrosion [41]. Figure 2 demonstrates Nyquist plots for mild steel in blank solution and several concentrations of MPBS at 30 °C. It shows one part of semicircles with one capacitive loop that increases in diameter in the presence of the tested compound. The EIS parameters, including charge-transfer reluctance (R_{ct}), double-layer capacitance (C_{dl}), and corrosion repression efficacy (ηI, %), are analyzed using an equivalent circuit model as shown in the inset of Fig. 2 and listed in Table 3. ηI and C_{dl} are calculated using Eqs. (12), (13)[42].

$$\eta I(\%) = \theta \times 100 = \left[\frac{R_{ct(uninh)} - R_{ct(inh)}}{R_{ct(uninh)}}\right] \times 100 \tag{12}$$

$$C_{dl} = \left(Y_0 R_{ct}^{1-n}\right)^{\frac{1}{n}} \tag{13}$$

where $R_{ct(inh)}$ and $R_{ct(uninh)}$ are the charge-transfer resistance in the case of with and without of MPBS inhibitor, Y_0 and n are the constant phase element (CPE) and the CPE directrix, respectively.

Table 3 illustrates that R_{ct} increases while C_{dl} reduces in the existence of the corrosion inhibitor. The R_{ct} increment with the growth of corrosion inhibitor concentration is due to the growth of the electrical double-layer thickness as a result of the gradual replacement of water on the mild steel surface by adsorbed corrosion inhibitor molecules [43]. The reduction in C_{dl} and the expansion in electrical double-layer thickness confirm the inhibitor's adsorption on both anodic and cathode sites [44].

Adsorption isotherm

The adsorption of corrosion inhibitor at the exterior metal boundary exemplifies the first stage in the inhibition process.

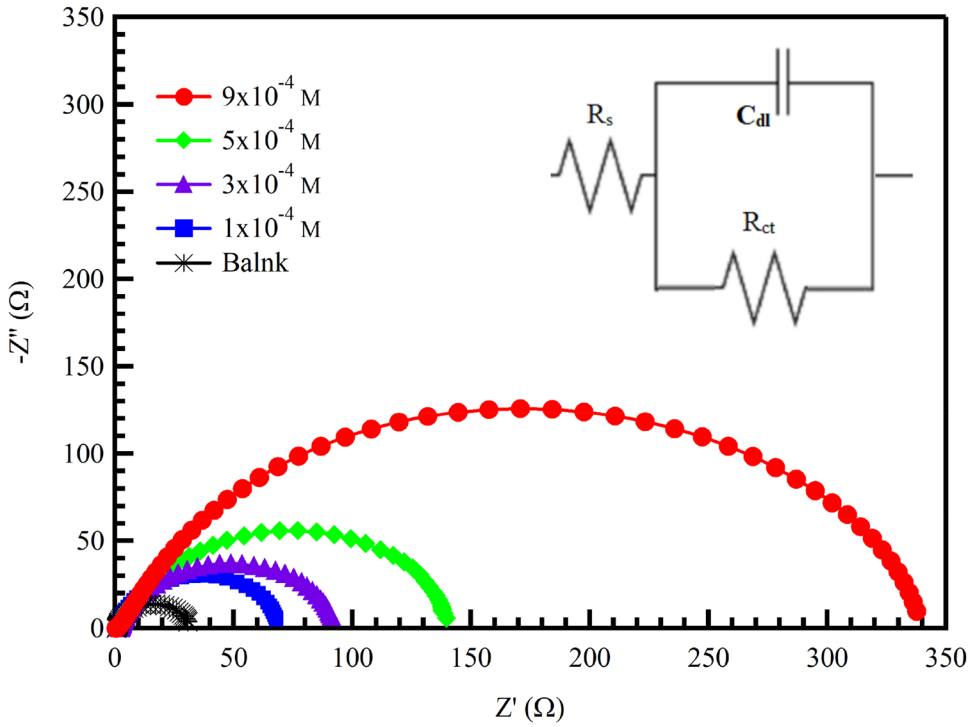

Fig. 2 Nyquist plots and the equivalent circuit (inset) used to fit the impedance data for mild steel in 1.0 mol/L H_2SO_4 solutions containing various MPBS inhibitor concentrations at 30 °C

Table 3 Impedance data for mild steel in 1.0 mol/L H_2SO_4 solution containing various concentrations of the MPBS inhibitor at 30 °C

Test solution	Conc. (M)	R_{ct} (Ω cm^2)	Y_0 (μF/cm^2)	n	Surface coverage (θ)	ηI (%)	C_{dl} (μF/cm^2)
Blank	–	28.96	203.2	0.98	-	-	185.24
MPBS	1×10^{-4}	64.44	108.7	0.98	0.55	55.06	97.98
	3×10^{-4}	92.29	157	0.86	0.69	68.62	78.26
	5×10^{-4}	139.5	129.3	0.86	0.79	79.24	68.58
	9×10^{-4}	327.3	47.55	0.83	0.91	91.15	20.55

Calculation of adsorption isotherm is essential to comprehend the interface between MPBS as a corrosion inhibitor and the exterior-metal surface in blank solutions. It is observed that adsorption of the corrosion inhibitor on the mild steel external surface complies with Langmuir isotherm as follows:

$$\frac{\theta}{1-\theta} = K_{ads}C \tag{14}$$

where K_{ads}, C, and θ are the adsorption constant, corrosion inhibitor concentration, and the exterior surface exposure/coverage obtained from the potentiodynamic measurements, respectively. Figure 3 shows that the excellent fitted straight line was achieved from the scheme of C/θ versus C. The correlation factor (R^2) was employed to select the isotherm most excellent fit with the experimental findings. The adsorption free energy ΔG°_{ads} was calculated based on Eq. (15) [45].

$$\Delta G_{ads} = -2.303\left(RT\log\left(55.5K_{ads}\right)\right) \tag{15}$$

where T is the temperature (K), and the value 55.5 refers to the molar-concentration of water. The negative value of ΔG_{ads} indicated that the adsorption operation willingly processes and steadiness of the formed layer-shield on the mild steel exterior surface [46]. In general, values from – 20 up and – 40 kJ/mol of ΔG_{ads} are harmonious with the electrostatic attraction between the corrosion inhibitor and the charged metal-surface (physically-adsorption). Extra-negative values of ΔG_{ads} suggest the sharing or shift of electrons from the corrosion inhibitor to the metal exterior surface to create a real coordinate chemical bond (chemically-adsorption) [47]. Based on Fig. 3, ΔG°_{ads} value was found to be − 10.20 kJ/mol, which is proportionate with the physical adsorption of the corrosion inhibitor on the mild steel exterior surface.

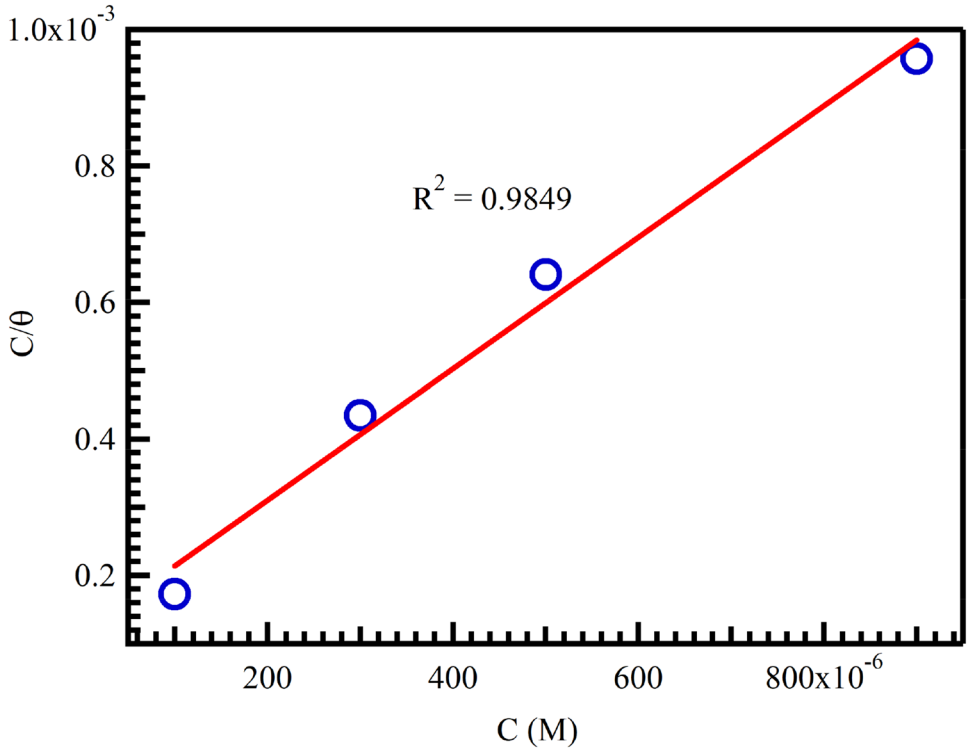

Fig. 3 Langmuir adsorption plot for mild steel in 1.0 mol/L H_2SO_4 solution containing various concentrations of the MPBS inhibitor at 30 °C

Morphological investigations

The SEM micrograph outlines the exterior surface of mild steel, as illustrated in Fig. 4a. The micrograph of the mild steel top-view surface demonstrated an uncompromising attack after dipping in the blank solution for one day, in which situation the external surface seemed to be cruelly harmed due to a few fractures and pits as a result of the offensive of corrosive medium. On the other hand, after inundation in 1.0 mol/L H_2SO_4 solution for 24 h and the presence of the corrosion inhibitor (9×10^{-4} M, MPBS, Fig. 4b), SEM image displayed the creation of dense adsorbed layers on the exterior surface of mild steel and a lessening in surface coarseness associated to the external surface of blank, mild steel as revealed in Fig. 4a. It has been proved that there is an effective defensive outer-layer of the proposed corrosion inhibitor adsorbed on the mild steel outer-surface. That adsorbed MPBS outer layer is answerable for the safeguard against the corrosion process of the mild steel surfaces.

Quantum chemical calculations

Optimized geometries of MPBS and its distributions HOMO, LUMO are shown in Fig. 5a. It could be observed that MPBS has a similar distribution of HOMO and LUMO. The HOMO and LUMO of MPBS corrosion inhibitor are found mainly around the (C, N, and O) moiety. The existence of N and O atoms on these molecules, along with many π-electrons, guarantees high adsorption of the corrosion inhibitor on the mild steel external surface. In Table 4, the decrease in value of EL, as well as the increase in the value of E_{HOMO}, reflects an increase in inhibitor efficiency. The high value of E_{HOMO} corresponds to the propensity of the molecule to provide electrons and the higher inhibition behavior for the metal.

In contrast, the low value of E_{LUMO} demonstrates the predisposition of the molecule to receive a lone pair of electrons [48]. The lower value of the energy gap ($\Delta E = E_{LUMO} - E_{HOMO}$) will result in excellent inhibition efficiency. From Table 4, it has been shown that inhibition efficiency will be high due to the low value of hardness equal to 0.781 eV and the high value of softness [49]. The electrophilicity index of MPBS was found to be 61.871 eV, which confirms the high inhibition efficiency. The efficiency of inhibition increases due to the high value of the dipole moment, depending on the type and nature of the molecules employed. Adsorption may be increased by the elevated value of 9.094 Debye. Therefore, it is possible to protect the mild steel surface. Moreover, Table 4 shows that the high total energy (TE) value (− 2367.68 a.m.u) indicates the molecule higher stability, and therefore, its propensity to donate potential is lower [50, 51]. In Lukovits's study, the inhibition efficacy increases by boosting the electron-providing capability of the corrosion inhibitor on the exterior metal surface, where the value of ΔN is less than 3.6 [51]. The MPBSΔN considerable value of 0.32 eV shows the maximum electron transfer and the higher efficiency of inhibition.

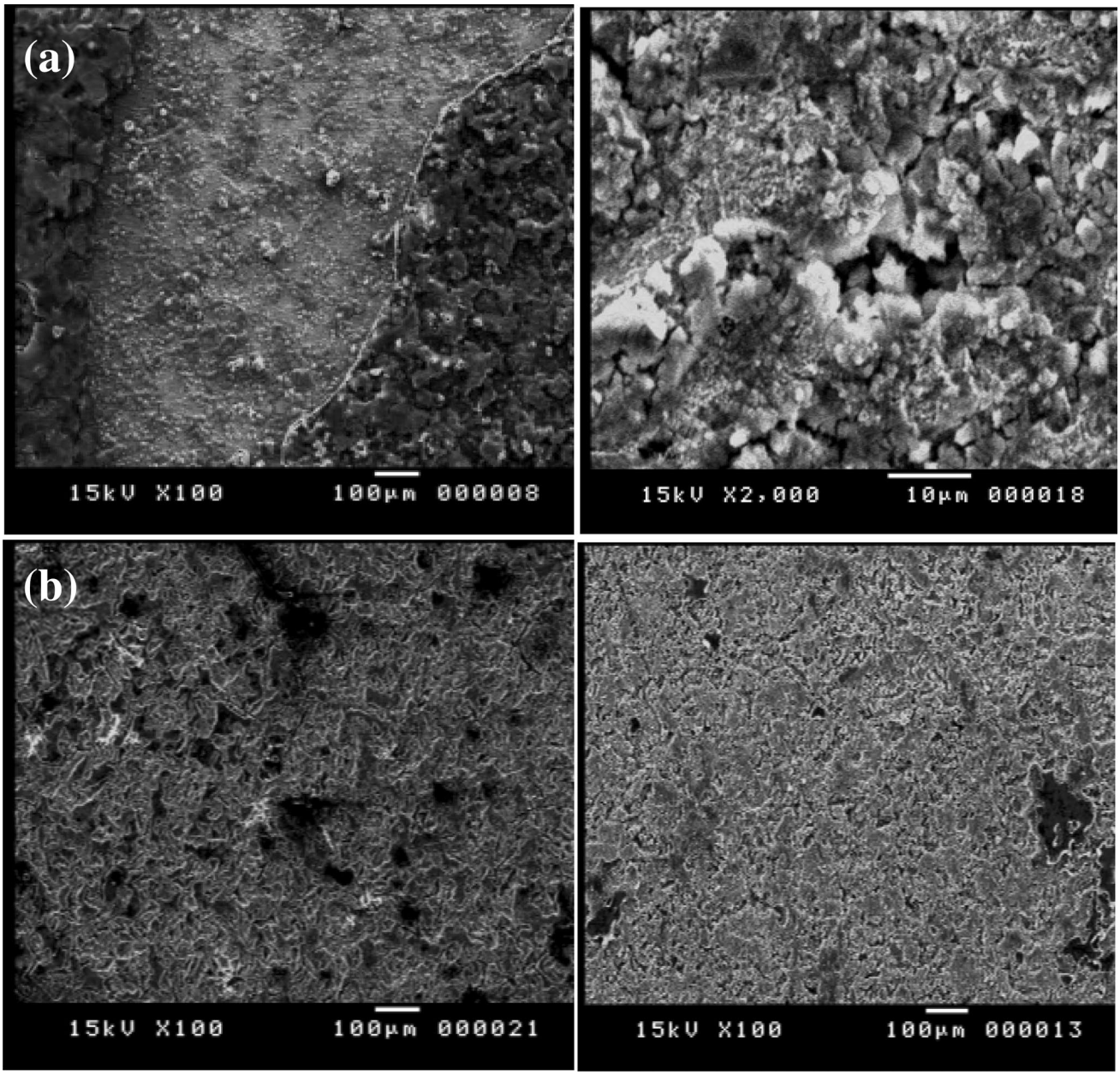

Fig. 4 SEM images of mild steel surface after 1 day immersed in 1.0 mol/L H_2SO_4 at room temperature in the absence (**a**) and existence (**b**) of MPBS inhibitor

The determination of active sites on inhibitors is essential to the mechanism of corrosion. Among essential parameters for determining active inhibitor-sites are molecular electrostatic potential (MEP) maps and MEP contours. The MEP has been utilized to define the electrophilic and nucleophilic locations on the molecule. The negative (red) regions and the positive (blue) regions of MEP indicate nucleophilic and electrophilic reactivity, respectively. The blue color regions prefer to interact with the electron-rich locations of specific chemical species such as metals, while red color regions prefer to interact with electron-poor locations of the metal surface, according to Fig. 5b, the blue color around the C atom of C=O group in which the pentadactyl chain is attached is dominated; hence this C atom has electrophilic reactivity. Mulliken population assessment was used to assess the adsorption addresses of corrosion inhibitor and the calculations of the charge spreading over the whole scope of the molecule skeleton [52]. In Table 5, the computed Mulliken negative charges of chosen atoms (carbon, oxygen, and nitrogen) are presented. Therefore, they preferred

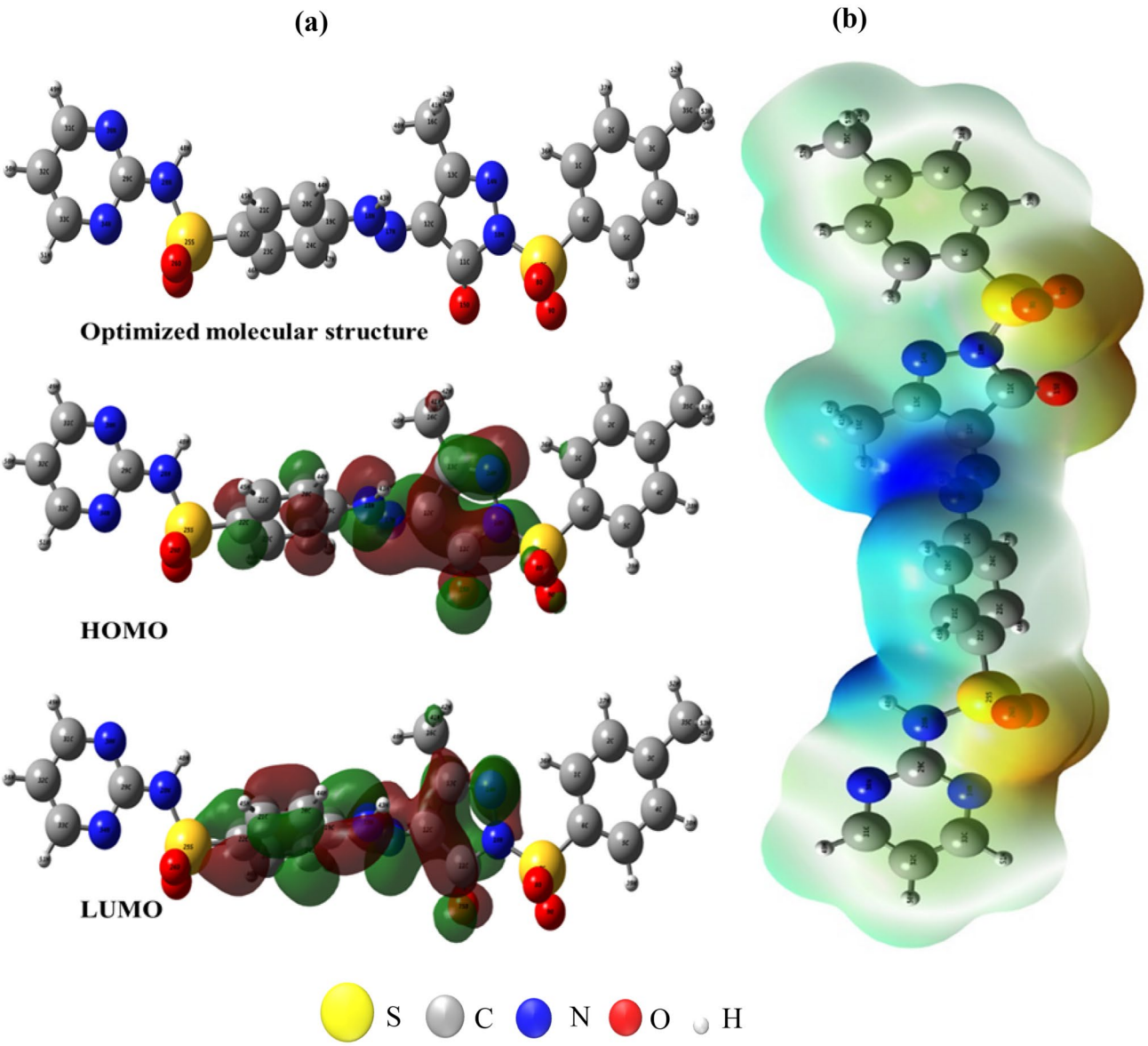

Fig. 5 The optimized molecular structure HOMO and LUMO (**a**), and the total charge density (**b**) of the investigated MPBS using density functional theory 6-311G (*d*, *p*) basis set method

Table 4 The calculated theoretical chemical parameters of MPBS at B3LYP/6-311G (*d*, *p*) basis set method

E_{HOMO} (ev)	E_{LUMO} (ev)	ΔE (ev)	H (ev)	σ (ev)	ω (ev)	Dm (Debye)	TE (a.m.u)	ΔN (ev)
− 7.731	− 6.169	1.561	0.781	1.281	61.871	9.094	− 2367.68	0.32

adsorption sites on a mild steel external surface [53]. The contours of the MEP shown in Fig. 5b are red, which is associated with negative charges. The steric effect can be seen in the MEP contour. From the contour of the MEP, the O atom of the other C=O group common to all inhibitors is the active site with less steric effect.

Mechanism of inhibition

The zero-charge potential of mild steel in acidic solutions is reported to be positive [54]. Therefore, the SO_4^{2-} ions are electrostatically attracted to the metal surface, creating a layer of negative charges. This will favor the adsorption of MPBS on the surface and thus reduce the dissolution of mild

Table 5 Calculated Mulliken atomic charges of the MPBS inhibitor

Atom Mulliken charges								
$-C_1$	$-C_2$	$-C_3$	$-C_4$	$-C_5$	$-C_6$	$-O_8$	$-O_9$	$-N_{10}$
0.035967	0.059084	0.102230	0.064834	0.016288	0.303827	0.472345	0.482399	0.483010
$-C_{12}$	$-N_{14}$	$-O_{15}$	$-C_{16}$	$-N_{17}$	$-N_{18}$	$-C_{20}$	$-C_{21}$	$-C_{22}$
0.149598	0.207937	0.263181	0.267277	0.09993	0.241440	0.120357	0.015801	0.383642
$-C_{23}$	$-C_{24}$	$-O_{26}$	$-O_{27}$	$-N_{28}$	$-N_{30}$	$-C_{32}$	$-N_{34}$	$-C_{35}$
0.017488	0.097619	0.476997	0.482445	0.565337	0.361149	0.234510	0.341910	0.255044

steel. In addition to this electrostatic attraction between the azopyrazole-benzenesulfonamide derivative and the metal exterior-surface, the obtained ΔG_{ads} value is consistent with physical adsorption mode. Nevertheless, the existence of lone pairs of electrons and benzene rings may promote the adsorption process. There may still be a chance for the formation of coordination bonds by the lone pair of electrons and some vacant orbits for metal. However, owing to the obtained results, such a combination is expected to occur on a small scale. The results indicated that the inhibition efficiency was excellent. This could be explained in view of the molecular structures of the tested compound. Thus, the presence of benzene rings, N, O, and S in the MPBS structure promotes its inhibitive action.

Conclusion

The experimental and theoretic findings indicate that the azopyrazole-benzenesulfonamide derivative (MPBS) works at room temperature as an efficient corrosion inhibitor of mild steel corrosion in 1.0 mol/L H_2SO_4 with maximal inhibition proficiency (93.61%). The values of inhibition efficacy rise with the growth of corrosion inhibitor concentration. The MPBS compound's adsorption on a mild steel exterior-surface of 1.0 mol/L H_2SO_4 is a physical phenomenon indicated by the values of (ΔG_{ads}) obtained and observed by the Langmuir isotherm. SEM analyzed the surface morphology and gave a tangible idea and real perception about creating a shielding layer on the exterior surface of mild steel, which reduces the corrosion level. Some chemical quantum factors have been calculated to interpret the inhibition mechanism further. The parameters were noticed to be close to the inhibition efficiencies of the corrosion resistance established.

References

1. D.D.N. Singh, T.B. Singh, B. Gaur, Corros. Sci. **37**(6), 1005 (1995)
2. N.H. Abu Bakar, G.A.M. Ali, J. Ismail, H. Algarni, K.F. Chong, Prog. Org. Coat. **134**, 272 (2019)
3. N. Asadi, M. Ramezanzadeh, G. Bahlakeh, B. Ramezanzadeh, J. Taiwan Inst. Chem. Eng. **95**, 252 (2019)
4. S. John, R. Jeevana, K.K. Aravindakshan, A. Joseph, Egypt. J. Pet. **26**(2), 405 (2017)
5. B.M. Prasanna, B.M. Praveen, N. Hebbar, T.V. Venkatesha, H.C. Tandon, Int. J. Ind. Chem. **7**(1), 9 (2015)
6. V. Hemapriya, P. Saranya, K. Parameswari, S. Chitra, Int. J. Curr. Eng. Technol. **4**(6), 3844 (2014)
7. A.S. Fouda, M.A. Elmorsi, T. Fayed, I.A. El Said, Desalin. Water Treat. **57**(10), 4371 (2014)
8. M. Bouchouit, M.E. Said, M.K. Ali, S. Bouacida, H. Merazig, N.K. Chaouche, A. Chibani, B. Zouchoune, A. Belfaitah, A. Bouraiou, Polyhedron **119**, 248 (2016)
9. F. Bisceglie, G. Del Monte, P. Tarasconi, G. Pelosi, Inorg. Chim. Acta **434**, 143 (2015)
10. S.M.A. Hosseini, A. Azimi, I. Sheikhshoaei, M. Salari, J. Iran. Chem. Soc. **7**(4), 799 (2010)
11. A. Kamal, A.B. Shaik, N. Jain, C. Kishor, A. Nagabhushana, B. Supriya, G. Bharath Kumar, S.S. Chourasiya, Y. Suresh, R.K. Mishra, A. Addlagatta, Eur. J. Med. Chem. **92**, 501 (2015)
12. S. Yamamoto, H. Kobayashi, T. Kaku, K. Aikawa, T. Hara, M. Yamaoka, N. Kanzaki, A. Hasuoka, A. Baba, M. Ito, Biorg. Med. Chem. **21**(1), 70 (2013)
13. H.A. Abdel-Aziz, K.A. Al-Rashood, K.E.H. ElTahir, G.M. Suddek, Eur. J. Med. Chem. **80**, 416 (2014)
14. R.M. Kubba, A.S. Alag, Int. J. Sci. Res. **6**(6), 1832 (2017)
15. N. Singh, A. Pandurangan, K. Rana, P. Anand, A. Ahamad, A.K. Tiwari, Int. Curr. Pharm. J. **1**(5), 110 (2012)
16. R. Touir, R. Belakhmima, M.E. Touhami, L. Lakhrissi, M. El Fayed, B. Lakhrissi, E. Essassi, J. Mater. Environ. Sci. **4**(6), 921 (2013)
17. N.S. Patel, S. Jauhari, G.N. Mehta, B. Hammouti, S.S. Al-Deyab, M. Bouachrine, J. Iran. Chem. Soc. **9**(5), 635 (2012)
18. I.O. Arukalam, Pigm. Resin Technol. **43**(6), 394 (2014)
19. M. Sikine, Y.K. Rodi, H. Elmsellem, O. Krim, H. Steli, Y. Ouzidan, A.K. Rodi, F.O. Chahdi, N. Sebbar, E. Essassi, J. Mater. Environ. Sci. **7**, 1386 (2016)
20. L. Toukal, S. Keraghel, F. Benghanem, A. Ourari, Int. J. Electrochem. Sci. **13**, 951 (2018)
21. A. Sayed, I.M.M. Othman, M. Hamam, H. Gomaa, M.I. Gadallah, M.A. Mostfa, H.R.H. Ali, M.Y. Emran, M. Abdel-Hakim, M.H. Mahross, J. Mol. Struct. **1225**, 129175 (2021)
22. S. Sardar, T. Akhtar, S. Hameed, K.M. Khan, J. Chem. Soc. Pak. **34**(6), 1531 (2012)
23. M. El-Sabbah, H. Khalil, M. Mahross, B. Mahran, A. Gomaa, Molecules **1**, 2 (2015)
24. A. Nagiub, F. Mansfeld, Corros. Sci. **43**(11), 2147 (2001)
25. M. Saraçoğlu, M.I.A. Elusta, S. Kaya, C. Kaya, F. Kandemirli, Int. J. Electrochem. Sci. **13**, 8241 (2018)
26. Z. Salarvand, M. Amirnasr, M. Talebian, K. Raeissi, S. Meghdadi, Corros. Sci. **114**, 133 (2017)
27. P. Dohare, K.R. Ansari, M.A. Quraishi, I.B. Obot, J. Ind. Eng. Chem. **52**, 197 (2017)
28. F. Tezcan, G. Yerlikaya, A. Mahmood, G. Kardaş, J. Mol. Liq. **269**, 398 (2018)

29. O.A.A. El-Shamy, M.I. Nessim, Tenside, Surfactants, Deterg. **54**(5), 443 (2017)
30. S. Kaya, B. Tüzün, C. Kaya, I.B. Obot, J.Taiwan Ins. Chem. Eng. **58**, 528 (2016)
31. M. Mahross, A. Naggar, T.A.S. Elnasr, M. Abdel-Hakim, Chem. Adv. Mater. **1**(1), 6 (2016)
32. J. Tang, H. Wang, X. Jiang, Z. Zhu, J. Xie, J. Tang, Y. Wang, M. Chamas, Y. Zhu, H. Tian, Int. J. Electrochem. Sci. **13**, 3625 (2018)
33. O. Fergachi, F. Benhiba, M. Rbaa, R. Touir, M. Ouakki, M. Galai, B. Lakhrissi, H. Oudda, M.E. Touhami, Mater. Res. **21**(6), e20171038 (2018)
34. G. Kavitha, S. Jegannathan, C. Vedhi, Int. J. ChemTech Res. **7**, 1693 (2015)
35. M.S.S. Adam, A.D.M. Mohamad, Polyhedron **151**, 118 (2018)
36. M. Mishra, K. Tiwari, A.K. Singh, V.P. Singh, Inorg. Chim. Acta **425**, 36 (2015)
37. F.B. Ravari, A. Dadgareenezhad, J. Chil. Chem. Soc. **58**(3), 1853 (2013)
38. D. Jayaperumal, Mater. Chem. Phys. **119**(3), 478 (2010)
39. N. Obi-Egbedi, K. Essien, I. Obot, E. Ebenso, Int. J. ChemTech Res. **6**, 913 (2011)
40. D.M. Gurudatt, K.N. Mohana, H.C. Tandon, Mater. Discov. **2**, 24 (2015)
41. R. Kashkovskiy, K. Strelnikova, A. Fedotova, Corros. Eng., Sci. Technol. **54**(6), 493 (2019)
42. M. Yadav, S. Kumar, I. Bahadur, D. Ramjugernath, Int. J. ChemTech Res. **9**(2014), 6529 (2014)
43. R. Govindasamy, S. Ayappan, J. Chil. Chem. Soc. **60**(1), 2786 (2015)
44. F.M. Mahgoub, B.A. Abdel-Nabey, Y.A. El-Samadisy, Mater. Chem. Phys. **120**(1), 104 (2010)
45. G.A.H. Gouda, G.A.M. Ali, T.A. Seaf Elnasr, Int. J. Nanomater. Chem. **1**(2), 39 (2015)
46. H. Zarrok, R. Salghi, A. Zarrouk, B. Hammouti, H. Oudda, L. Bazzi, L. Bammou, S. Al-Deyab, Der. Pharm. Chem. **4**(1), 407 (2012)
47. C. Verma, J. Haque, E.E. Ebenso, M.A. Quraishi, Results Phys. **9**, 100 (2018)
48. E. Ilham, A. Boutouil, H. Ben El Ayouchia, M.R. Laamari, M. El Haddad, H. Anane, S. Salah-Eddine, Prot. Metals Phys. Chem. Surf. **55**(1), 166 (2019)
49. A. Aouniti, H. Elmsellem, S. Tighadouini, M. Elazzouzi, S. Radi, A. Chetouani, B. Hammouti, A. Zarrouk, J. Taibah Univ. Sci. **10**(5), 774 (2016)
50. C. Verma, L.O. Olasunkanmi, I.B. Obot, E.E. Ebenso, M.A. Quraishi, RSC Adv. **6**(59), 53933 (2016)
51. J. Haque, C. Verma, V. Srivastava, M.A. Quraishi, E.E. Ebenso, Results Phys. **9**, 1481 (2018)
52. E.E. Ebenso, K. Khaled, S.K. Shukla, A.K. Singh, N. Eddy, M. Saracoglu, L.C. Murulana, F. Kandemirli, T. Arslan, I. Obot, Int. J. Electrochem. Sci. **7**, 5643 (2012)
53. O. Mahmoudi, T. Bordjiba, A.M. Affoune, Int. J. Electrochem. Sci. **11**, 4427 (2016)
54. P. Dohare, D.S. Chauhan, A.A. Sorour, M.A. Quraishi, Mater. Discov. **9**, 30 (2017)

Affiliations

M. A. Mostfa[1] · H. Gomaa[1] · Ismail M. M. Othman[1] · Gomaa A. M. Ali[1]

✉ Gomaa A. M. Ali
gomaasanad@azhar.edu.eg

H. Gomaa
gomaa.h1989@gmail.com

[1] Chemistry Department, Faculty of Science, Al-Azhar University, Assiut 71524, Egypt